IUST
Iran University of Science and Technology

Iranian Journal of Electrical and Electronic Engineering

Journal Homepage: ijeee.iust.ac.ir

Research Paper

Non-Linearity Effects of Industrial Loads on Induction Motor Servo Drive System

H. Azizi Moghaddam*(C.A.), A. Farhadi**, and S. Mohamadian***

Abstract: In the new advanced drive schemes, identification and modeling of the load complex characteristics can play an important role to predict the dynamic performance of the proposed control strategy. The novelty of this paper consists in the classification of the different types of the nonlinear loads which the electrical drive systems may encounter. In this study, nonlinear components of mechanical loads are divided into two groups. The first type includes nonlinear phenomenon caused by the nature of load which is predictable and identifiable. Another type of loads nonlinear characteristic happens due to the occurrence of a mechanical fault in motor, coupling or load parts. Generally, this type of non-intended nonlinear effect is not predictable and often occurs in the installation and operation stage of the drive system utilization. In this paper, the performance of an induction servo drive system has been simulated under the influence of different types of non-linear industrial loads.

Keywords: Backlash Unbalancing, Crankshaft Mechanism, Multi Mass System, Non-Linear Load, Servo Drive.

1 Introduction

THE emergence of modern control strategies such as neural networks, sliding mode, and predictive control methods has attracted the attention of researchers in the last few decades to develop servo drive systems. These methods have the main feature of being robust against the uncertain and nonlinear dynamics of the drive system [1-4]. Therefore, for theoretical and experimental evaluation of a new control strategy, the complicated and non-linear load behaviors should be considered. Generally, for laboratory studies, the dynamometers are versatile and ideal for mechanical load emulation. Although various dynamometer test equipment has been developed in recent years [5-7], they are not capable of emulating all these complicated behaviors.

In order to evaluate the load torque of an electrical drive, four regions should be considered in the torque-speed characteristic of the system [8]. A typical torque-speed characteristic of a drive system is shown in Fig. 1. As can be seen, the drive can operate the electrical machine as either a motor or a generator. In transient or

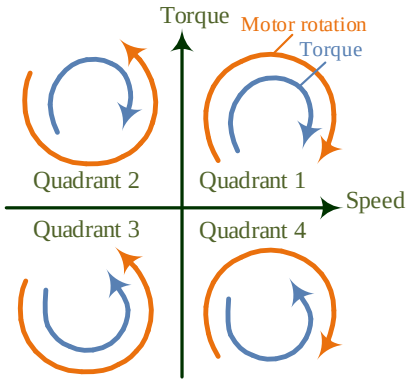

Fig. 1 The torque-speed characteristic of a drive system.

Iranian Journal of Electrical and Electronic Engineering, 2022.
Paper first received 01 December 2020, revised 28 October 2021, and accepted 04 November 2021.
* The author is with the Rotating Electrical Machines Research group, Niroo Research Institute, Tehran, Iran.
E-mail: hmoghaddam@nri.ac.ir.
** The author is with the Department of Electrical and Computer Engineering, K. N. Toosi University of Technology, Tehran, Iran.
E-mail: farhadi@email.kntu.ac.ir.
*** The author is with the School of Engineering, Damghan University, Damghan, Iran.
E-mail: s.mohamadian@du.ac.ir.
Corresponding Author: H. Azizi Moghaddam.
https://doi.org/10.22068/IJEEE.18.2.2046

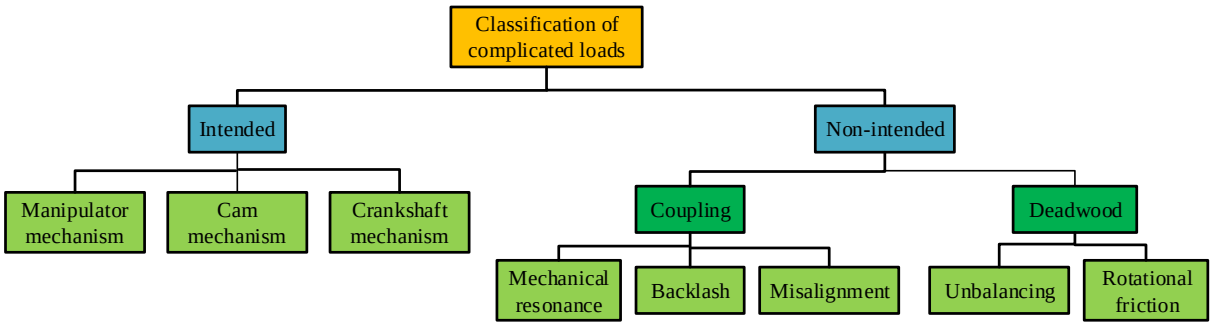

Fig. 2 Classification of complicated mechanical loads in servo drive systems.

steady-state conditions, the operating point location is entirely determined based on the load type.

In a conventional classification, load torques can be divided into six categories based on the behavior of the torque versus speed, position, or time [9] as follow:

- **Constant:** Load torque is independent of the speed. For example, Coulomb friction and conveyors.
- **Frictional:** Load torque is linearly proportional to speed. For example, viscous friction.
- **Quadratic:** Load torque is proportional to the **square** of speed. For example, fan and pump applications.
- **Constant power:** Load torque is in the reverse proportion of speed with a constant power. For example, milling machines.
- **Path-dependent:** Load torque depends on the behavior of the path tracked by the load during its motion. For example, transport systems and planning machines.
- **Rotor angle-dependent:** Load torque is a function of rotor angle. For example, reciprocating compressors.

It is evident that several other complicated and non-linear mechanical loads have not been taken into consideration. In this paper, different nonlinear behaviors of mechanical loads are investigated in the servo drive system. It is proposed to classify non-linear load torques into two categories as intended and non-intended. The proposed classification of mechanical loads is shown in Fig. 2. An intended non-linear load torque is provided to perform beneficial mechanical works. This torque, being predictable and repeatable, converts a rotational movement into a transmission movement or vice versa, by using a designed mechanism. On the other hand, non-intended load torques, resulting in either the faults of the coupling system or deadwood torques, occur via the interaction between the intended load and unwanted non-predictable events.

In addition to recognition and classification of the loads complicated and nonlinear behaviors, one of the main objectives of this paper is to study the requirements necessary to enable a modern dynamometer system with a large bandwidth to emulate the load high-frequency torque components

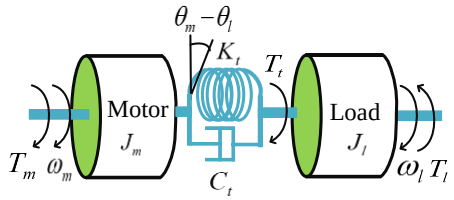

Fig. 3 Mechanical model of a two-mass system.

experimentally. Various non-linear characteristics of well-known industrial mechanical loads will be investigated in the following sections through mathematical modeling and simulation results.

2 Mathematical Models of Drive System

A motor-load set, considered absolutely rigid, can be modeled as a rotational complex known as a one-mass model which is described with the following basic equation [10]:

$$T_m = J\dot{\omega} + T_l \tag{1}$$

where J, T_m, and T_l are the total moment of inertia, the motor, and load torques, respectively. The angular position of the system can be denoted as $q = wt$. As in (1), the motor torque, T_m, must oppose two torques which are the static torque T_l and the dynamic torque $J\dot{\omega}$.

In a large number of electrical drives, the motor is commonly coupled to the load with flexible transmission systems such as gears, shafts, and belts. These systems are called two-mass systems and their mechanical model is shown in Fig. 3. The dynamical equation of a two-mass system is described as [11]

$$\begin{cases} J_m\dot{\omega}_m = T_m - T_t \\ J_l\dot{\omega}_l = T_t - T_l \\ T_t = K_t\left(\theta_m - \theta_l\right) + C_t\left(\omega_m - \omega_l\right) \end{cases} \tag{2}$$

where J_m and J_l are the inertia moment of the motor and load, respectively. T_t is the transmission system torque. C_t and K_t are the damping and stiffness factors of the transmission system, respectively. q_l and q_m are the angular positions of the load and rotor, respectively. Also, the angular speeds of the motor and the load are denoted as $\omega_m = \dot{\theta}_m$ and $\omega_l = \dot{\theta}_l$, respectively.

In some applications, the transmission system may have several inertias. Hence, the dynamic equation of the system should be arranged according to a multi-mass model. However, a two-mass model as in (2) has been considered in this paper in order to describe the mathematical equations of coupling non-intended loads. Due to the fact that the torque of intended and deadwood non-intended loads has complicated equations, the effect of damping and stiffness of the transmission system are neglected and the motor-load set is assumed similar to a one-mass system expressed in (1). In the next sections, the mathematical model of loads is obtained for each case and the response of the drive system will be simulated. An induction motor controlled by a field-oriented method is used in all simulations. Parameters of the simulated motor-load network are listed in Table A1 of Appendix.

3 Coupling Non-Intended Loads

3.1 Mechanical Resonance

The rotational parts of an electric drive inherently produce a mechanical resonance leading to unwanted noise, high stressed, crashing of the system's different parts, and so on [12]. Inflexible transmission systems, the motor-load set is faced with a mechanical fluctuation due to the resonance between the elasticity of the transmission system and the inertia of the motor and the load [13]. This resonance can be treated as coupling non-intended load. In order to investigate the effect of the resonance, the state-space equations of (2) should be described first as [14]

$$\dot{x}=\underbrace{\begin{bmatrix} -\frac{C_t}{J_m} & \frac{C_t}{J_m} & -\frac{K_t}{J_m} \\ \frac{C_t}{J_l} & -\frac{C_t}{J_l} & \frac{K_t}{J_l} \\ 1 & -1 & 0 \end{bmatrix}}_{A} x+\underbrace{\begin{bmatrix} \frac{1}{J_m} \\ 0 \\ 0 \end{bmatrix}}_{B_u} T_m+\underbrace{\begin{bmatrix} 0 \\ -\frac{1}{J_l} \\ 0 \end{bmatrix}}_{B_w} T_l \tag{3}$$

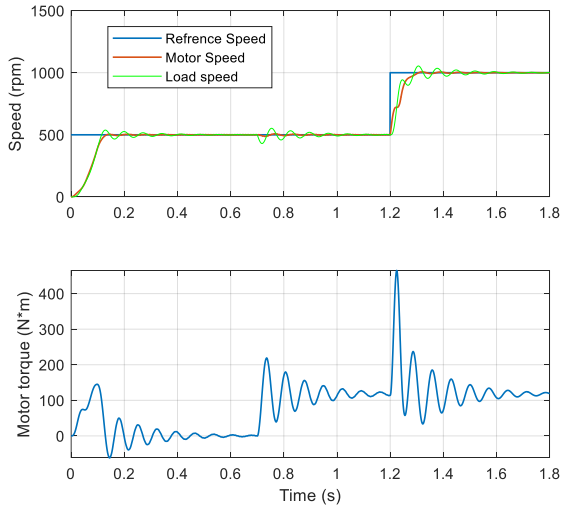

Fig. 4 The shaft speed and torque for K_t = 1500 Nm/rad.

where $x = [w_m\ w_l\ q_t]^T$ in which $q_t = q_m - q_l$. The input-to-output transfer function of the system of equations in (3) $T_m w_m$ can be written as

$$\frac{\omega_m(s)}{T_m(s)}=\begin{bmatrix}1 & 0 & 0\end{bmatrix}(sI-A)^{-1}B_u = \frac{1}{s}\times\frac{s^2+\frac{C_t}{J_l}s+\frac{K_t}{J_l}}{J_m\left(s^2+C_t\left(\frac{1}{J_m}+\frac{1}{J_l}\right)s+K_t\left(\frac{1}{J_m}+\frac{1}{J_l}\right)\right)} \tag{4}$$

If the damping factor C_t is neglected, the anti-resonance f_{ares} and resonance frequencies f_{res} will be

$$\begin{cases} f_{ares}=\dfrac{1}{2\pi}\sqrt{\dfrac{K_t}{J_l}} \\ f_{res}=\dfrac{1}{2\pi}\sqrt{K_t\left(\dfrac{1}{J_m}+\dfrac{1}{J_l}\right)} \end{cases} \tag{5}$$

According to (5), K_t, J_m, and J_l affect the resonance phenomenon. In order to show their influence, simulation studies are carried out on the motor described in Table A1 of Appendix. In simulations, a flexible shaft is considered as the coupling non-intended load and the reference speed is changed at t = 1.2 s. A constant load torque is applied to the motor at t = 0.7 s. the results for rotor speed and T_m are shown in Fig. 4 and Fig. 5 for K_t = 1500 N.m/rad and K_t=15000 N.m/rad, respectively, where the effect of resonance in torque and speed fluctuations is evident during transient intervals Based on these figures, larger fluctuations occur in the case of smaller shaft stiffness factor,. Also, the effect of two other parameters, i.e., J_m and J_l, is simulated and similar results are obtained. Therefore, it is necessary to consider the mechanical resonance phenomenon in the controller so as to eliminate its effect.

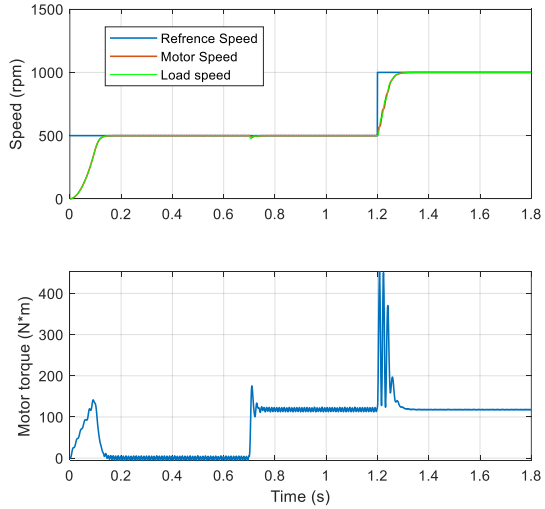

Fig. 5 The shaft speed and torque for K_t =15000 Nm/rad.

3.2 Backlash

The rotational parts of an electric drive system inherently produce a mechanical resonance called backlash, leading to unwanted issues such as noise, high stresses, and crashing some parts of the system. The backlash phenomenon can be mentioned as a nonlinear behavior occurred by loose motion in some coupling systems such as gear systems and chain drives [15]. In other words, backlash is caused by the dead zone region created due to the gap between input and output positions of the transmission system [16]. The backlash phenomenon inappropriately affects the stability in limited cycles, deteriorates the system performance, and it can be a disadvantageous fault when constant speed is demanded [17]. Considering gap α in a two-mass system shown in Fig. 6, the transmission system torque of (2) should be modified as [18]

$$T_t = K_t\left(\theta_t - \theta_b\right) + C_t\left(\dot{\theta}_t - \dot{\theta}_b\right) \tag{6}$$

where q_b is the backlash angle. The derivative of the backlash angle is expressed by

$$\dot{\theta}_b = \begin{cases} \max\left(0, \dot{\theta}_b + \dfrac{K_t}{C_t}\left(\theta_t - \theta_b\right)\right), & \theta_b = -\alpha \\ \dot{\theta}_b + \dfrac{K_t}{C_t}\left(\theta_t - \theta_b\right), & \left|\theta_b\right| < \alpha \\ \min\left(0, \dot{\theta}_b + \dfrac{K_t}{C_t}\left(\theta_t - \theta_b\right)\right), & \theta_b = \alpha \end{cases} \tag{7}$$

If the damping factor C_t is ignored, the torque of the transmission system will change to the dead-zone model written as

$$T_t = K_t D_\alpha, \qquad D_\alpha = \begin{cases} \theta_b - \alpha, & \theta_b = -\alpha \\ 0, & \left|\theta_b\right| < \alpha \\ \theta_b + \alpha, & \theta_b = \alpha \end{cases} \tag{8}$$

Considering the dead-zone model (8) for the transmission torque, Figs. 7 and 8 show the simulation results of a shaft connected to the load by gear gap angles α = 1° and α = 5°, respectively. When motor speed is changing (the transient period in Figs. 7 and 8 for the real speed to settle to its reference), the motor gear impacts the load gear where each strike imposes a torque spike on the motor accelerating the speed of the system. The wider the gear gap angle, the higher the motor torque spike of the motor and it may damage the shaft. The simulation results show that the backlash phenomenon occurs only in transient conditions. Therefore, in some drive systems such as elevators that require a soft start with minimum vibrations or fluctuations, the control system must be designed to reduce this effect.

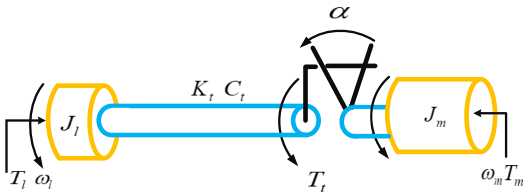

Fig. 6 The model of a two-mass system with backlash effect.

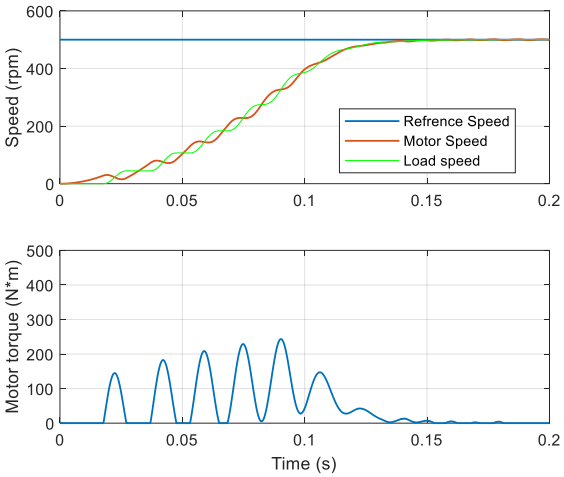

Fig. 7 The shaft speed and torque for K_t = 1500 Nm/rad.

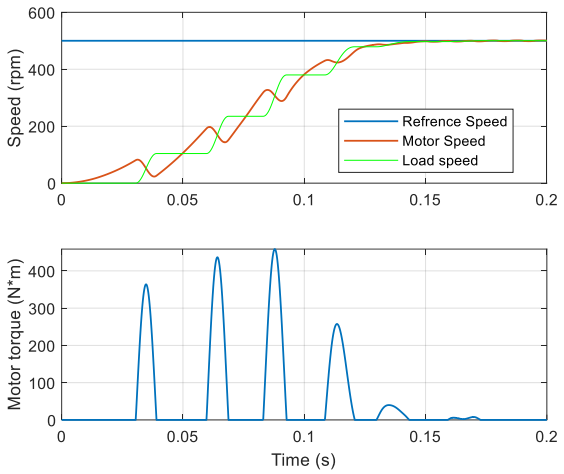

Fig. 8 The shaft speed and torque for K_t = 15000 Nm/rad.

3.3 Misalignment

Misalignment is the most common problem in the performance of electric drive systems, especially in machine trains [19]. Misalignment leads to reactionary forces in the shaft which causes premature failures and vibration. This difficulty could occur in three different formations including parallel, angular or combined as reported in [20]. To summarize the mathematical description of misalignment, only the angular type will be presented. Fig. 9 shows the mechanical model of angular misalignment of two shafts connecting the motor and load together like a universal joint with an intersection angle *b*.

Mathematical representation of the speed of two shafts in Fig. 9 is given as follows [21]:

$$\frac{\omega_l'}{\omega_l}=\frac{\cos(\beta)}{1-\sin^2(\beta)\sin^2(\theta_l)} \tag{9}$$

where w'_l is the shaft speed on the side joined to the load. The above equation can be approximated in two terms being a constant term and an oscillating term having twice the frequency of the system speed [21]. As the mechanical power of the shaft of the motor side $T_t w_m$ is similar to that of the other side $T'_t w'_m$, the torques relationship can be described as

$$\frac{T_t'}{T_t}=\frac{1-\sin^2(\beta)\sin^2(\theta_l)}{\cos(\beta)} \tag{10}$$

If the above equation is decomposed, an oscillating component at twice the frequency of the system speed can be observed. Therefore, the dynamic equation of (2) can be modified as follows:

$$\begin{cases} J_m\dot{\omega}_m=T_m-T_{tt}' \\ J_l\dot{\omega}_l=T_t-T_l \\ T_t'=K_t(\theta_m'-\theta_l)+C_t(\omega_m'-\omega_l) \end{cases} \tag{11}$$

In order to show the effect of the misalignment, simulation results are provided in Fig. 10 for a load having a shaft connected to the shaft of a motor by an intersection angle of 5°. As seen in Fig. 10, the motor torque has fluctuations in the steady-state where the amplitude of fluctuations increases as the speed increases. The frequency spectrum of motor torque is presented in Fig. 11. As expected, the torque ripple frequency appears at 36 Hz that is almost twice the frequency of the system speed (1000 rpm) at 16.67 Hz.

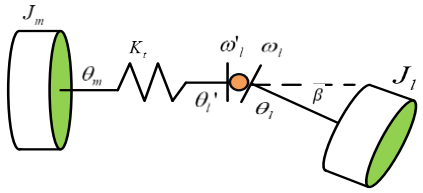

Fig. 9 Motor-load system with flexible shaft modeled as a universal joint.

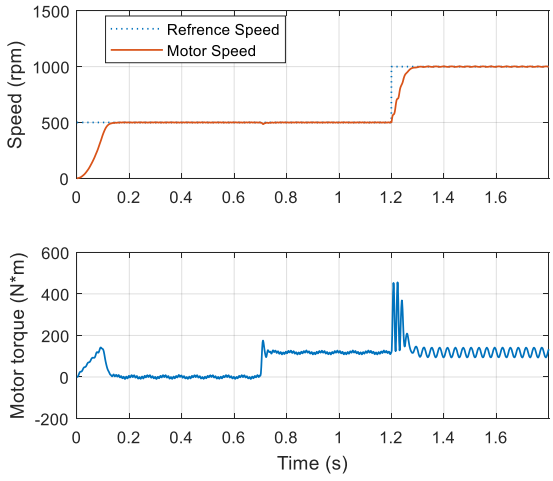

Fig. 10 The shaft speed and torque for angular misalignment.

4 The Deadwood Non-Intended Loads

4.1 Unbalancing

Manufacturers of industrial drive systems try to assemble all mechanical parts of the drive without unbalancing. However in practice, due to the faults happening in the manufacturing process such as the non-uniform density of the material, tolerances on mating parts, distributed unbalance in a long slender shaft and etc., the rotor of the motor or the transmission system can be inevitably unbalanced [22]. In this situation, the center of mass of rotating parts is not matched with the center of rotation that causes synchronous vibration in drive systems [23]. Suppose a mass m_u placed at an interval r_u from the center of mass of rotating parts as shown in Fig. 12. The unbalanced torque T_u caused by the tangential force F_t of the weight of the mass, reported in [24], is described as

$$T_u=r_uF_t=m_ugr_u\cos(\theta) \tag{12}$$

where g is gravitational acceleration. As it can be seen, the torque T_u appears as an oscillatory term at a frequency of rotation. In addition, the mass of the unbalanced load produces an inertia expressed as $J_u = m_u r_u^2$. Hence, the second line of (1) should be modified by

$$T_m=(J+J_u)\dot{\omega}+T_u+T_l \tag{13}$$

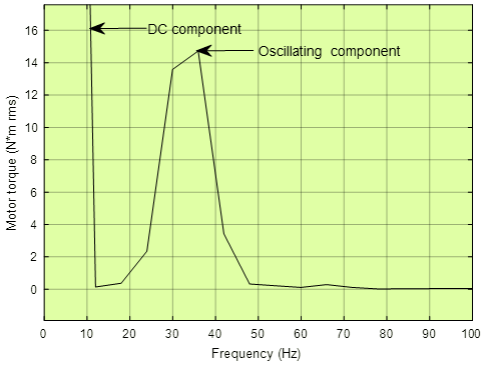

Fig. 11 Frequency spectrum of motor torque for the angular misalignment of coupling in the speed of 1000 rpm.

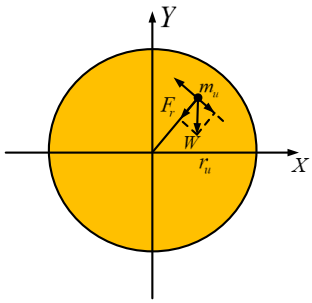

Fig. 12 Model of an unbalanced load.

The results for a motor-load system with a mass m_u =3 Kg placed at a distance r_u =25 cm from the center of mass of rotating parts are shown in Fig. 13. The motor torque oscillates in the steady-state whose amplitude increases as the speed increases. Based on the frequency spectrum shown in Fig. 14, the torque oscillation frequency (17 Hz) almost equals to the frequency of the system speed (1000 rpm) at 16.67 Hz.

4.2 Rotational Friction

The rotational friction torque caused by friction in contact with the relative motions of body drive almost occurs in all of the industrial drive systems such as brakes, drive belting, wheel or rail, etc. [25, 26]. This torque resists the motion and damages the surface of system components. The rotational friction torque is defined as the sum of a linear (being the viscous friction torque) and non-linear, (involving Coulomb T_c and break-away T_b torques) components of speed, described as [27]

$$T_f = B_l + \left(T_c + \left(T_b - T_c\right)e^{-\left(-\omega/\omega_b\right)^2}\right)\text{sign}\left(\omega\right) \quad (14)$$

where T_f, w_b, and B_l are the rotational friction torque, break-away speed threshold, and the viscous friction coefficient of the load, respectively. Therefore, the torque T_f must be added to (1) when there is rotating friction in the system.

The simulation results for the friction torque and the speed of a drive system, having Coulomb torque T_c = 20 N.m, break-away torque T_b = 25 N.m, break-away speed threshold w_b = 1 rad/s, and viscous friction coefficient B_l = 0.1 are illustrated in Fig. 15. A negatively sloped torque due to a non-linear component of rotational friction is presented in the motor torque at low speeds. At the steady-state, a constant torque caused by the sum of Coulomb and the viscous friction torques is observable as in Fig. 15.

5 Intended Loads

5.1 Manipulator Mechanism

Manipulators are one of the most significant mechanisms in manufacturing and industrial automation. Manipulator mechanisms are generally used to enhance performance characteristics such as speed, repeatability, and accuracy. In addition, they can be employed to replace manual workers in dangerous environments for routine works [28, 29]. Manipulators can have a complicated structure with several links and arms. In order to simplify the description of the dynamic equation of a manipulator, a conventional two-link manipulator is shown in Fig. 16.

In Fig. 16, l_1 and d_1 are the length of the first link and the distance from the gravity center of the first link to point O_1, respectively. Similarly, l_2 and d_2 are the length of the second link and the distance from the gravity center of the second link to point O_2, respectively. The equation of motion for the two-link manipulator, reported in [30], is given as

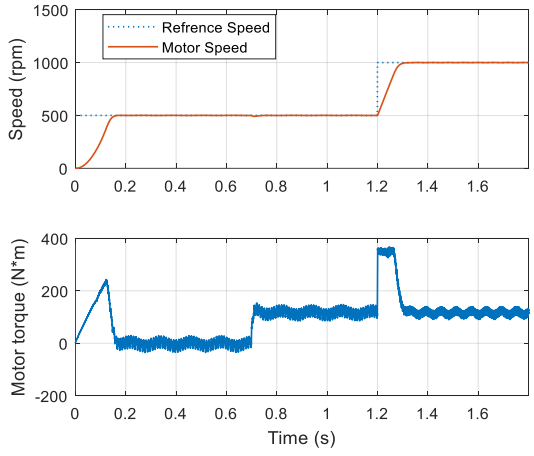

Fig. 13 Motor speed and torque for unbalanced load.

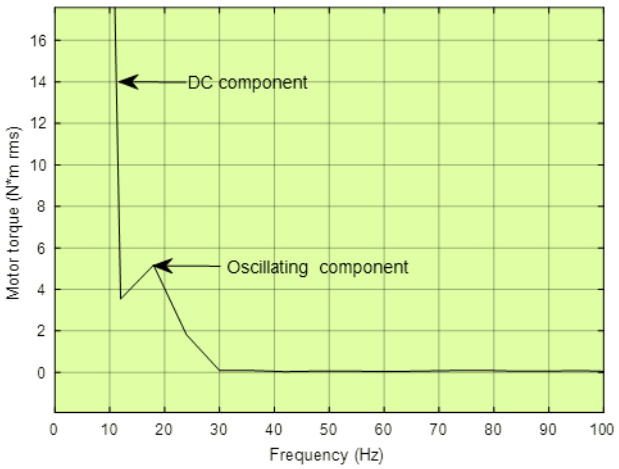

Fig. 14 Frequency spectrum of motor torque with unbalanced load at the speed of 1000 rpm.

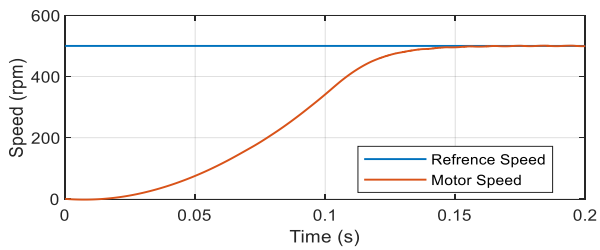

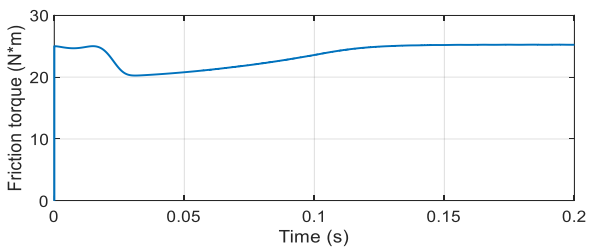

Fig. 15 Motor speed and torque for unbalanced load.

$$\begin{bmatrix} T_{m1} \\ T_{m2} \end{bmatrix} = \begin{bmatrix} D_{11} & D_{12} \\ D_{21} & D_{22} \end{bmatrix} \begin{bmatrix} \ddot{\theta}_1 \\ \ddot{\theta}_2 \end{bmatrix} + \begin{bmatrix} C_1 \\ C_2 \end{bmatrix} + \begin{bmatrix} G_1 \\ G_2 \end{bmatrix} \tag{15}$$

where T_{m1} and T_{m2} are the torque of motors applied at O_1 and O_2, respectively. The angular position of the first and the second links are q_1 and q_2, respectively. Other parameters are defined as

$$\begin{cases} D_{11} = J_1 + J_2 + m_2 l_1^2 + 2m_2 l_1 d_2 \cos(\theta_2) \\ D_{12} = D_{21} = J_2 + m_2 l_1 d_2 \cos(\theta_2) \\ D_2 = J_2 \\ C_1 = -m_2 l_1 d_2 \sin(\theta_2)\left(\dot{\theta}_2 + 2\dot{\theta}_1\dot{\theta}_2\right) \\ C_2 = m_2 l_1 d_2 \sin(\theta_2)\dot{\theta}_1^2 \\ G_1 = g\left(m_1 d_1 + m_2 l_1\right)\cos(\theta_1) + g m_2 d_2 \cos(\theta_1 + \theta_2) \\ G_2 = g m_2 d_2 \cos(\theta_1 + \theta_2) \end{cases} \tag{16}$$

where m_1 and m_2 are the mass of the first link and the second link, respectively. The parameters J_1 and J_1 are the moment of inertia about an axis through the center of mass of the first link and the second link, respectively.

In order to show the operation of the system under a two-link manipulator, a simulation for the drive system joined to the first link of the manipulator is done. The parameters of the manipulator are expressed in Table A2 of Appendix and the simulation results are shown in Fig. 17. In this scenario, the second link rotates with another drive system that the angle of the second link is changed from 60 to 30 degrees and then rotates from the angle of 30 degrees to 15 degrees at the time of 1.3s. At times 0.7s to 0.8s, the drive system produces a non-linear torque having a sinusoidal form to rotate the first link from 0 degrees to 45 degrees. At time 1s to 1.1s, the second link imposes a non-linear torque with a sinusoidal form to the first link when reduces its angle. At time 1.1s to 1.3s, the angles of both links are changed that caucuses the torque response different from the torque response at time 0.7s to 0.8s. All of these non-linear torque components have roots in the non-linear equation of motion as expected from (15).

5.2 Cam Mechanism

A cam mechanism, including two links: a cam and a follower, converts a rotational movement of the cam into a determined reciprocating movement of the follower or vice versa [31]. Cam is one of the most important mechanisms in industrial machinery such as screw machines, gear-cutting machines, textile machinery, and printing presses [32]. An eccentric cam mechanism, reported in [33], consisting of a plate with a camshaft, a follower mass, and a maintaining spring is shown in Fig. 18.

If the motor joined at point "O", the load torque, mentioned in (1), is defined as follows:

$$T_l = F_c d_c \sin(\theta) = d_c\left(K_f d_c + P\right)\sin(\theta) + \frac{1}{2} d_c^2\left(m_c\omega^2 - K_f\right)\sin(2\theta) \tag{17}$$

where d_c is the distance between the center of the plate and the center of the camshaft, respectively. The parameters K_f, m_c, and P are the stiffness of the spring, the mass of the follower, and the preload force of the spring, respectively.

Simulation results for an eccentric cam with parameters defined in Table A3 of Appendix are shown in Fig. 19. The torque of the motor has a harmonic form that its amplitude increases with increasing speed. This is because of (17) from which an oscillating frequency (36 Hz) at twice the motor speed frequency (16.67 Hz) is expected as shown in Fig. 20.

5.3 Crankshaft Mechanisms

Crankshaft mechanisms transform rotational motion to a reciprocating motion or vice versa with four

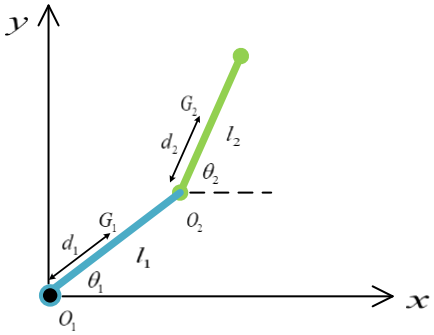

Fig. 16 A two-link manipulator schematic.

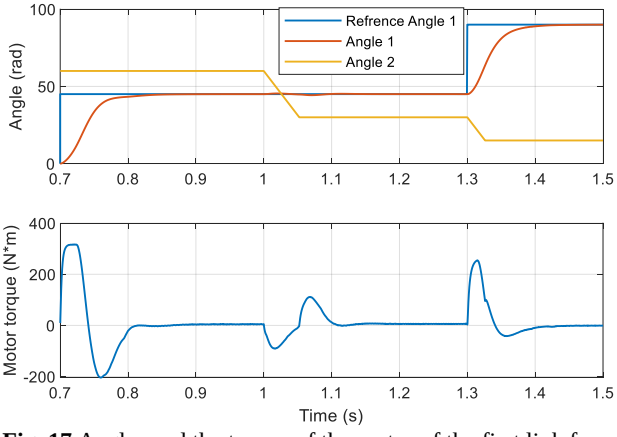

Fig. 17 Angles and the torque of the motor of the first link for the two-link manipulator.

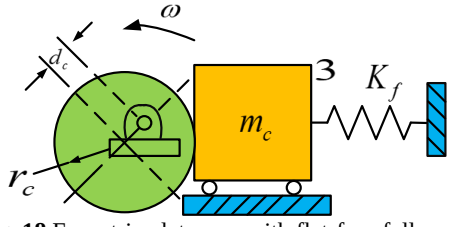

Fig. 18 Eccentric plate cam with flat-face follower.

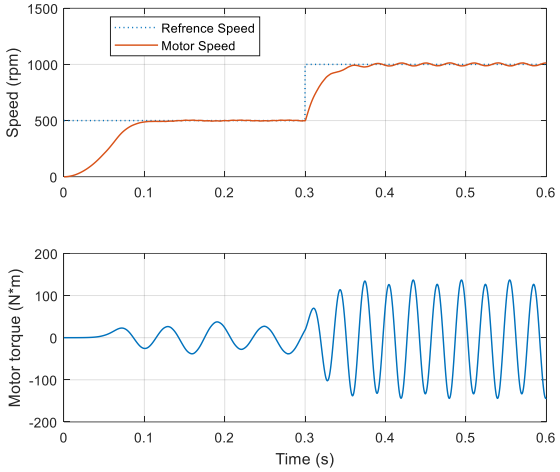

Fig. 19 The speeds and torque for the cam mechanism.

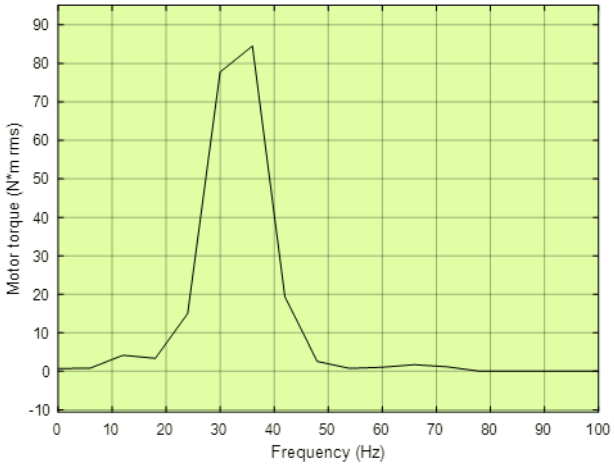

Fig. 20 Frequency spectrum of the motor torque for the assumed cam at the speed of 1000 rpm.

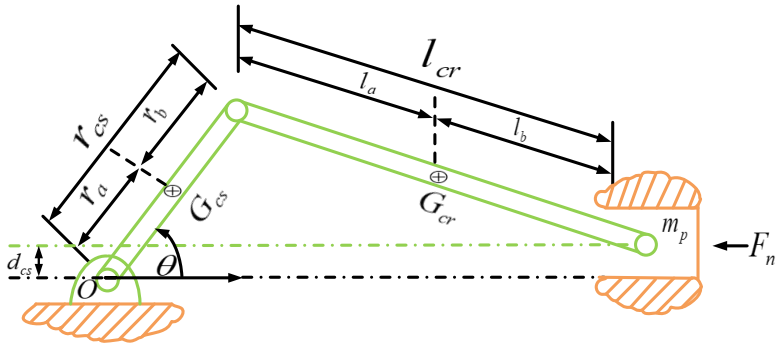

Fig. 21 Eccentric plate cam with flat-face follower.

components. A crankshaft mechanism is extensively used in compressors, weaving looms, rocking pumps, etc. [34]. The equivalent model of a vertical crankshaft mechanism is shown in Fig. 21 that it consists of a crank, an electric motor connected to the crank at point "O", a connecting rode, and a piston. The place of gravity center of the crank and the connecting rode is located at the center of their length that it divides the lengths into two parts "a" and "b" as shown in Fig. 21.

According to [35] the motor torque, mentioned in (1), is modified as the functions of the motor position given as

$$T_m = \left(J + J_{cs}(\theta)\right)\dot{\omega} + F_n r_{cs}\left(\sin(\theta) + \frac{\frac{r_{cs}}{l_{cr}}\sin(2\theta)}{\sqrt{1-\left(\frac{r_{cs}}{l_{cr}}\sin(2\theta)\right)^2}}\right) \quad (18)$$

where r_{cs}, l_{cr}, and F_n are the crank length, the connecting rod length, and normal force (which can be seen in the gas force of a compressor), respectively. $J_{cs}(q)$ is the inertia moment of the crankshaft mechanism around the point "O". If the inertia moment of the connecting rod around G_{cr} (the gravity center of the connecting rod) is assumed $J_{Gcr}=m_{cr}l_a l_b$, $J_{cs}(q)$ can be approximated as

$$J_{cs}(\theta) = J_{G_{cs}}(\theta) + \frac{m_{cr}l_b}{l_{cr}}r_{cs}^2 + \left(\frac{m_{cr}l_a}{l_{cr}} + m_p\right)r_{cs}^2 f(\theta) \quad (19)$$

where m_{cr}, m_p, and J_{Gcs} are the connecting rod mass and the piston mass, respectively. The inertia moment of the crank around the center of gravity G_{cs} is $J_{Gcs}=m_{cs}r_a r_b$ that m_{cs} is the mass of the crank. $f(q)$ is defined as

$$f(\theta) = \left(\sin(\theta) + \frac{\frac{r_{cs}}{2l_{cr}}\sin(2\theta) - \frac{d_{cs}}{l_{cr}}\cos(\theta)}{\sqrt{1-\left(\frac{r_{cs}}{l_{cr}}\sin(\theta) - \frac{d_{cs}}{l_{cr}}\right)^2}}\right) \quad (20)$$

If the vertical crankshaft mechanism with the parameters illustrated in Table A4 of Appendix is used, the torque and speed of the system will be simulated as shown in Fig. 22. The torque has a little ripple before 0.65s due to the first term of (18). When the normal force is applied at 0.65s, the torque has an oscillating form whose frequency is increased as the speed increases. The torque has two main components, shown in the second term of (20), at once and twice the frequency of the speed that can be seen in the frequency spectrum of the torque in Fig. 23.

6 Conclusion

In the current research, different types of torque of the

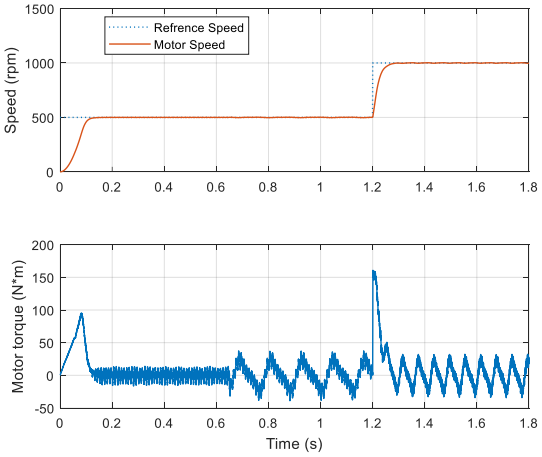

Fig. 22 The speed and torque for the crankshaft mechanism.

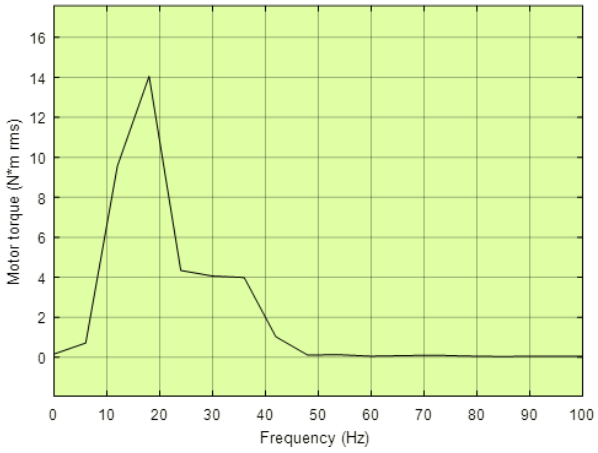

Fig. 23 Frequency spectrum of the motor torque for the crankshaft mechanism at the speed of 1000 rpm.

Table A1 Motor parameters.

Parameter	Symbol	Value
Nominal power	P_n	50 hp
Nominal voltage	V_n	400 V
Nominal frequency	f_n	50 Hz
Pole pairs	p	2
The inertia moment of motor	J_m	0.18 kg.m^2
The inertia moment of load	J_l	0.18 kg.m^2

Table A2 Parameters of the two-link manipulator.

Parameter	Symbol	Value
The mass of first link	m_1	5 kg
The mass of second link	m_2	5 kg
The length of first link	l_1	50 cm
The length of second link	l_2	50 cm
The distance from the center of the first link	d_1	25 cm
The distance from the center of the second link	d_2	25 cm
The moment of inertia of the first link	J_1	0.18 kg.m^2
The moment of inertia of the second link	J_2	0.18 kg.m^2

non-linear loads were studied and the dynamic behavior of the drive system under the influence of the load non-linear components was analyzed and simulation results were presented. According to the results obtained in this research, it can be said that the non-linear loads are divided into two groups of intended and non-intended loads. The torque of non-intended loads was either caused by coupling system errors such as backlash or the torques existing in the nature of load such as friction. At the time of designing the drive system, the effect of non-intended non-linear loads on system performance should be predicted to avoid the occurrence of costly damages. As presented in simulation results, backlash and mechanical resonance problems are capable of creating significant fluctuations in response to torque and leading to serious errors in the drive system. The difference between the torque of intended nonlinear loads and other introduced loads is that the mechanical load mechanism is designed in a way that the load torque applied to the drive system creates a non-linear and complex behavior. Therefore, it is better to study the effect of these mechanisms on drive system response before using them so that the required observances can be performed to design torque and speed controllers. In practice, the concomitant combinations of different nonlinear loads are possible in which various combinations can be applied to the simulation model based on the equations presented in this paper in order to analyze the system behavior. In fact, the mutual effect between different load types entails modeling and analysis of mechanical behavior which can be considered in future studies. In order to exactly investigate the effect of non-linear dynamics of the load on servo system behavior, it is required to assess the function of control methods under the influence of these phenomena in a laboratory environment. Design and construction of wide bandwidth and very high response speed dynamometer system can make it possible to exactly investigate the non-linear dynamics of the load and design control systems resistant to these components in the laboratory environment.

Appendix

The parameters of the induction motor used for simulations are listed in Table A1 and the mechanical parameters of some loads, described within the paper, are indicated in Tables A2 to A4.

Table A3 Parameters of the cam mechanism.

Parameter	Symbol	Value
The distance between the center of the plate and the center of the camshaft	d_c	5 cm
The stiffness of the spring	K_f	1500 N.m/rad
The mass of follower	m_c	10 Kg
The preload force of the spring	P	75 N.m

Table A4 Parameters of the vertical crankshaft mechanism.

Parameter	Symbol	Value
The crank length	r_{cs}	10 cm
The connecting rod length	l_{cr}	30 cm
The distance between the center of piston and the point "O"	d_{cs}	2 cm
The connecting rod mass	m_{cr}	3 Kg
The piston mass	m_p	1 Kg
The normal force	F_n	200 N

Intellectual Property

The authors confirm that they have given due consideration to the protection of intellectual property associated with this work and that there are no impediments to publication, including the timing of publication, with respect to intellectual property.

Funding

No funding was received for this work.

CRediT Authorship Contribution Statement

H. Azizi Moghaddam: Conceptualization, Methodology, Software, Formal analysis, review and editing. **A. Farhadi:** Software, Formal analysis, Writing -Original draft and editing. **S. Mohamadian**: Scientific review and Language editing.

Declaration of Competing Interest

The authors hereby confirm that the submitted manuscript is an original work and has not been published so far, is not under consideration for publication by any other journal and will not be submitted to any other journal until the decision will be made by this journal. All authors have approved the manuscript and agree with its submission to "Iranian Journal of Electrical and Electronic Engineering".

References

[1] A. Farhadi, A. Akbari, A. Zakerian, and M. Tavakoli Bina, "An improved model predictive control method to drive an induction motor fed by three-level diode-clamped indirect matrix converter," *International Journal of Engineering and Technology Innovation*, Vol. 10, No. 4, pp. 265–279, Sep. 2020.

[2] V. Naik N and S. P. Singh, "A novel interval type-2 fuzzy-based direct torque control of induction motor drive using five-level diode-clamped inverter," *IEEE Transactions on Industrial Electronics*, Vol. 68, No. 1, pp. 149–159, Jan. 2021.

[3] A. Farhadi, A. Zakerian, and A. Nazari, "Predictive control of neutral-point clamped indirect matrix converter," *Iranian Conference on Electrical Engineering (ICEE)*, pp. 1406–1411, May 2017.

[4] Q. Zou, L. Sun, D. Chen, and K. Wang, "Adaptive sliding mode based position tracking control for PMSM drive system with desired nonlinear friction compensation," *IEEE Access*, Vol. 8, pp. 166150–166163, Sep. 2020.

[5] M. Rodic, K. Jezernik, and M. Trlep, "Dynamic emulation of mechanical loads: an advanced approach," *IEE Proceedings – Electric Power Applications*, Vol. 153, No. 2, pp. 159–166, Mar. 2006.

[6] Z. Zhang, L. Wang, J. Zhang, and R. Ma, "Study on requirements for load emulation of the vehicle with an electric braking system," *IEEE Transactions on Vehicular Technology*, Vol. 66, No. 11, pp. 9638–9653, Nov. 2017.

[7] J. Song-Manguelle, G. Ekemb, D. L. Mon-Nzongo, T. Jin, and M. L. Doumbia, "A theoretical analysis of pulsating torque components in AC machines with variable frequency drives and dynamic mechanical loads," I*EEE Transactions on Industrial Electronics*, Vol. 65, No. 12, pp. 9311–9324, Dec. 2018.

[8] N. H. Fuengwarodsakul, M. Menne, R. B. Inderka, and R. W. De Doncker, "High-Dynamic four-quadrant switched reluctance drive based on DITC," *IEEE Transactions on Industry Applications*, Vol. 41, No. 5, pp. 1232–1242, Sep. 2005.

[9] S. K. Pillai, *A first course on electrical drives*. 1st ed. New Delhi: New Age International, 1990.

[10] K. Ohnishi, N. Matsui, and Y. Hori, "Estimation, identification, and sensorless control in motion control system," *Proceedings of the IEEE*, Vol. 82, No. 8, pp. 1253–1265, Aug. 1994.

[11] W. Leonhard, *Control of electrical drives*. 1st ed. Berlin: Springer, 2001.

[12] K. Szabat and T. Orlowska-Kowalska, "Vibration suppression in a two-mass drive system using PI speed controller and additional feedbacks—Comparative study," *IEEE Transactions on Industrial Electronics*, Vol. 54, No. 2, pp. 1193–1206, Apr. 2007.

[13] S. E. Saarakkala and M. Hinkkanen, "State-space speed control of two-mass mechanical systems: analytical tuning and experimental evaluation," *IEEE Transactions on Industry Applications*, Vol. 50, No. 5, pp. 3428–3437, Feb. 2014.

[14] D. H. Lee, J. H. Lee, and J. H. Ahn, "Mechanical vibration reduction control of two-mass permanent magnet synchronous motor using adaptive notch filter with fast Fourier transform analysis," *IET Electric Power Applications*, Vol. 6, No. 7, pp. 455–461, Aug. 2012.

[15] J. C. Conwell and G. E. Johnson, "Experimental investigation of link tension and roller-sprocket impact in roller chain drives," *Mechanism and Machine Theory*, Vol. 31, No. 4, pp. 533–544, May 1996.

[16] R. Merzouki, K. Medjaher, M. A. Djeziri, and B. Ould-Bouamama, "Backlash fault detection in mechatronic system," *Mechatronics*, Vol. 17, No. 6, pp. 299–310, Jul. 2007.

[17] M. Nordin and P.O. Gutman, "Controlling mechanical systems with backlash – A survey," *Automatica*, Vol. 38, No. 10, pp. 1633–1649, Oct. 2002.

[18] M. Calvini, M. Carpita, A. Formentini, and M. Marchesoni, "PSO-Based self-commissioning of electrical motor drives," *IEEE Transactions on Industrial Electronics*, Vol. 62, No. 2, pp. 768–776, Feb. 2015.

[19] A. W. Lees, "Misalignment in rigidly coupled rotors," *Journal of Sound and Vibration*, Vol. 305, No. 1–2, pp. 261–271, Aug. 2007.

[20] M. B. Deepthikumar, A. S. Sekhar, and M. R. Srikanthan, "Model based fault diagnosis of a rotor-bearing system for misalignment and unbalance under steady-state condition," *Journal of Sound and Vibration*, Vol. 327, No. 3–5, pp. 604–622, Nov. 2009.

[21] J. M. Bossio, G. R. Bossio, and C. H. De Angelo, "Angular misalignment in induction motors with flexible coupling," in *35th Annual Conference of IEEE Industrial Electronics*, Porto, pp. 1033–1038, Nov. 2009.

[22] D. G. Huang, "Characteristics of torsional vibrations of a shaft with unbalance," *Journal of Sound and Vibration*, Vol. 308, No. 3–5, pp. 692–698, Dec. 2007.

[23] H. Kim, "On-Line mechanical unbalance estimation for permanent magnet synchronous machine drives," *IET Electric Power Applications*, Vol. 3, No. 3, pp. 178–186, May 2009.

[24] U. B. Ferraz, P. F. Seixas, and W. E. Aguiar, "A simplified model for mechanical loads under angular misalignment and unbalance," *International Journal of Mechanical and Mechatronics Engineering*, Vol. 7, No. 7, pp. 1611–1617, Jan. 2013.

[25] D. Severin and S. Dörsch, "Friction mechanism in industrial brakes," *Wear*, Vol. 249, No. 9, pp. 771–779, Sep. 2001.

[26] T. H. C. Childs and D. Cowburn, "Contact observations on and friction of rubber drive belting," *Wear*, Vol. 100, No. 1-3, pp. 59–76, Dec. 1984.

[27] F. Marques, P. Flores, J.C. Pimenta Claro, and H. M. Lankarani, "A survey and comparison of several friction force models for dynamic analysis of multibody mechanical systems," *Nonlinear Dynamics*, Vol. 86, pp. 1407–1443, Aug. 2016.

[28] S. P. Patarinski and R. G. Botev, "Robot force control: A review," *Mechatronics*, Vol. 3, No. 4, pp. 377–398, Aug. 1993.

[29] K. C. Chiou and S. J. Huang, "An adaptive fuzzy controller for robot manipulators," *Mechatronics*, Vol. 15, No. 2, pp. 151–177, Mar. 2005.

[30] S. Oh and K. Kong, "Two-degree-of-freedom control of a two-link manipulator in the rotating coordinate system," *IEEE Transactions on Industrial Electronics*, Vol. 62, No. 9, pp. 5598–5607, Sep. 2015.

[31] H. J. Van de Straete and J. De Schutter, "Hybrid cam mechanisms," *IEEE/ASME Transactions on Mechatronics*, Vol. 1, No. 4, pp. 284–289, Dec. 1996.

[32] A. Torabi, S. Akbarzadeh, M. Salimpour, and M. M. Khonsari, "On the running-in behavior of cam-follower mechanism," *Tribology International*, Vol. 118, pp. 301–313, Feb. 2018.

[33] J. J. Dicker, G. R. Pennock, and J. E. Shigley, *Theory of machines*. 3rd ed. New York: McGraw-Hill, 2014.

[34] W. Li, Q. Yan, and J. Xue, "Analysis of a crankshaft fatigue failure," *Engineering Failure Analysis*, Vol. 55, pp. 139–147, Sep. 2015.

[35] B. Chen, Y. Wu, and F. Hsieh, "Estimation of engine rotational dynamics using Kalman filter based on a kinematic model," *IEEE Transactions on Vehicular Technology*, Vol. 59, No. 8, pp. 3728–3735, Oct. 2010.

H. Azizi Moghaddam received the B.Sc. degree in Electrical Engineering from Shiraz University, Shiraz, Iran, in 2001, and the M.Sc. and Ph.D. degrees in Electrical Engineering from Iran University of Science and Technology (IUST), Tehran, Iran, in 2004 and 2013, respectively. Currently, he is an Assistant Professor at the Rotating Electrical Machines group at Niroo Research Institute (NRI). His research interests include design and optimization of electrical machines, electrical machines drives and testing, and power electronics.

A. Farhadi received his master's degree in Engineer degree in Electrical Engineering from the Department of Electrical and Computer Engineering, K. N. Toosi University of Technology, Iran, in 2017. He is currently a Research Assistant with the Electrical Rotating Machines Research Department, Niroo Research Institute, Iran. His research interests include multilevel DC/AC converters, matrix converters, dynamometer systems, and model predictive control of power converters and drives.

S. Mohamadian received his B.Sc. and Ph.D. degrees in Electrical Engineering from Iran University of Science and Technology (IUST), Tehran, Iran, in 2007 and 2016, respectively. Between February 2014 and March 2015, he spent a period as a Visiting Scholar at the University of Trieste, Trieste, Italy, where he worked on research projects regarding high-power multiphase motor drives and multiphase machines modeling and analysis. In 2016, he joined the University of Damghan, Damghan, Iran, where he is currently an Assistant Professor. His research interests include power quality, power electronics, and electrical machines.